Disorder and order in sheared colloidal suspensions. II. Stochastic simulations

B. Morin and D. Ronis
Department of Chemistry, McGill University, 801 Sherbrooke Ouest, Montréal, Québec, Canada H3A 2K6
(Received 28 July 1998)

Motivated by predictions of previous theoretical work [B. Morin and D. Ronis, Phys. Rev. E **54**, 576 (1996)] we perform two dimensional stochastic simulations of sheared colloidal suspensions, governed by stochastic differential equations based on simple symmetries such as detailed balance (or time reversal symmetry of the action), which take the form of a modified fluctuating Navier-Stokes equation describing the local velocity of the fluid, coupled to a generalized convective-diffusion equation for the colloid number density. The results of the stochastic simulations are in agreement with earlier results based on the same model equations; specifically, there exists a transition in the homogeneous colloidal system to a layered phase at high shear rate and packing fraction. Additional insight is obtained through the analysis of the approximate equations for the first and second moments, derived perturbatively from the Fokker-Planck equation. [S1063-651X(99)14502-1]

PACS number(s): 82.70.−y, 64.60.My

I. INTRODUCTION

Rheology, the study of the properties of flowing materials, and, in particular, of flowing colloidal dispersions, has long been an area of active research. In practice, colloidal suspensions take many forms, such as paint, oil, grease, and even mud and foods such as sauces, among other things. The effect of shear on these systems is of practical interest since their fabrication and use often involve mixing of some sort. At the same time, the large variations in viscosity seen in these systems as a function of shear rate and concentration could be better exploited once a better understanding of the phenomena and of the role of the relevant parameters is reached.

Colloidal suspensions are comprised of microscopic particles, typically having a radius varying from 100 nm to 10,000 nm in magnitude. Because they exhibit all phases of condensed systems, i.e. gas, liquid, crystalline, and glass, they are ideal to study equilibrium and non-equilibrium aspects of phase transitions. Perhaps most important is their large diffusion time, τ_D, which makes colloidal dispersions very useful in the investigation of non-equilibrium phenomena, and more specifically, of the effects of applied shear stresses on liquids. For example, consider a colloidal particle with an effective diameter of $\sigma \sim 10^{-4}$ cm and with a diffusion constant $D_0 \sim 10^{-8}$ cm^2/s. The time for the colloidal particle to diffuse by a length σ is of the order of $\tau_D \sim \sigma^2/D_0 \sim 1$ s. Consequently, for concentrated suspensions, where the typical correlation length and inter-particle distance is $O(\sigma)$, the effects of a linear shear gradient are expected to manifest themselves once the shear rate, ω_0, is of the order of $1/\tau_D = 1$ s^{-1}, which is well within the range of experiments. Typical small molecule fluids on the other hand, have diffusion times 10^{10}–10^{12} times larger, thus requiring large shear rates, unreachable experimentally.

Earlier work by Hoffman [1] on crystalline phases of colloidal suspensions shows the typical phenomena seen in most such systems under shear; whether the equilibrium state is crystalline or liquid, the viscosity initially decreases (shear thinning), and then, in most cases, increases (shear thickening) before a (sometimes discontinuous) increase in viscosity is seen at large enough packing fractions. As the shear rate is increased past the shear thickening region (whether continuous or discontinuous), shear thinning resumes. Hoffman associated the discontinuity in viscosity to an order-disorder transition in which the system, originally crystalline, degenerates to a less ordered state. Liquid colloidal suspensions have the same behavior except that the discontinuous increase in viscosity is associated with an *increase* in order. Past the discontinuity, the system is thought to order into planes of colloid flowing with constant velocity over each other, thus reducing the viscosity as this new configuration allows for a flow with less collisions and/or hydrodynamic interactions between particles.

Nonequilibrium molecular dynamics simulations by Erpenbeck [2], Woodcock [3], Heyes, Morriss, and Evans [4], and Stevens, Robbins, and Belak [5], as well as nonequilibrium Brownian dynamics simulations by Xue and Grest [6] and Rastogi, Wagher, and Lustig [7], seem to confirm this scenario, although these simulations do not include the underlying solvent or concomitant hydrodynamic interactions. In addition, many of these simulations lead to what many consider an overly large ordered region in the shear rate versus volume fraction phase diagram. The work by Mitchell and Heyes [8] includes many-body hydrodynamics interactions in the Stokes approximation. The inclusion of these far-field hydrodynamics interactions do not reduce the size of the ordered region in the phase diagram, and may in fact promote the formation of layers. Hence, short-range hydrodynamics forces are thought to have an important role in building a realistic model for nonequilibrium simulations of colloidal suspensions.

The above calculations find instantaneous configurations that exhibit layering or string formation under shear. For example, the structure factors of Xue and Grest's develop large peaks in the neighborhood of the equilibrium main peak for wave vectors along the shear gradient direction, thereby signaling ordering in that direction at a particle separation close to the equilibrium average particle distance. For a certain range of shear rates, they also find a large peak in the structure factor for wave vectors along the vorticity direction (perpendicular to the flow and shear gradient direc-

 ©1999 The American Physical Society

tion) in the vicinity of the second peak of the equilibrium structure factor. This suggests further ordering in each plane into strings of particles, with strings in the plane above and below a reference plane (which flow at different velocities), staggered, in order to maximize the distance between strings of different velocities. Hence, strings form that are ordered in a triangular lattice in the plane perpendicular to the flow direction, while remaining disordered in the flow direction.

Both liquid and crystalline colloidal suspensions have roughly the same steady-state layered pattern which is more ordered than a liquid, but less ordered than a crystal, irrespective of whether the zero-shear equilibrium state was liquidlike or crystalline. In the presence of shear, the main difference is in the flow direction, where the crystal may remain crystalline (if somewhat less ordered), whereas the liquid remains disordered. Note, however, that flowing colloidal crystals can have long wavelength instabilities as the motion of a crystal plane with respect to another creates a periodic modulation of the elastic properties [9,10]. As a consequence, the existence of flowing crystals is limited by this phenomena, the details of which depend on the size and geometry of the system.

Hoffman's work also suggests that further increasing the shear rate after the jump in viscosity leads to a loss of order; the system becomes amorphous and then reorders weakly at even higher shear rates. Ackerson and co-workers [11] see much of the same behavior but are cautious about a simple interpretation of the weak order seen by Hoffman at the highest shear. Although light scattering might suggest a reappearance of order at very high shear rates, such evidence for reordering is not seen in neutron scattering. Consequently, other effects could be at the origin of the return of iridescence at very large shear rates, such as surface induced effects [11]. The instability mentioned at the end of the last paragraph is another possible explanation. In this work, we focus mostly on the transition to a layered state that probably corresponds to the resumption of shear thinning, past the shear thickening transition.

More recently, the hypothesis that an order-disorder transition is associated with a sudden increase in viscosity has been challenged [12]. It is suggested that the formation of layers is not necessary to the occurrence of shear thickening. In our view, this is right, but also consistent with the standard view. The shear thickening regime is a two-phase state where ''fluctuating'' layers coexist with the disordered state. Only at higher shear rates do steady-state layers form, thus reducing interparticle collisions and allowing shear thinning to resume. Hence, an order-disorder transition occurs not in the shear thickening regime, but at higher shear rates, at the onset of a second shear thinning regime.

In a previous work, [13], we performed a perturbative analysis of a model of colloidal suspensions which included hydrodynamic interactions associated with active mixing. The model equations were the same as those to be used here, and are described in the next section. It was found that the system responds nontrivially to the application of a linear shear gradient of the form: $\mathbf{v}_0=\omega_0 x\hat{\mathbf{y}}$, where ω_0 is the shear rate. For example, at zero wave number, the direct correlation function (and thereby the structure factor) increases as $\omega_0^{3/2}$ for small shear rates, whereas for sufficiently large wave numbers along the shear gradient direction (here k_x), i.e., for $k_x \gg (\omega_0\sigma)/D_0$ (where σ is the hard sphere particles' diameter, and D_0 is the diffusion constant), the nonequilibrium corrections to the structure factor has an ω_0^2 dependence, again for small shear rates. As the shear is increased, the structure factor evolves towards unity everywhere except in the plane $k_y=0$, i.e., perpendicular to the flow direction. In that special direction, the main peak initially decreases, and then increases with increasing shear until, for sufficiently high packing fraction, it diverges, suggesting the existence of long-range order at a finite wavelength, and presumably a lamellar pattern. A phase diagram in the packing fraction-shear rate plane was constructed having a line at a critical packing fraction below which no instability to the formation of layers exist even at infinite shear, and the spinodal-like line just described. Finally, it was found that the wavelength of the instability grows with the packing fraction. Motivated by these results, here we numerically perform two-dimensional stochastic simulations of Langevin equations describing the model in question, subjected to a linear shear gradient, and report on the results below.

In the next section, the model is presented together with some details relating to the stochastic simulation and a nonperturbative analysis based on moment equations. A numerical analysis of approximate equations governing the first and second moments is presented in Sec. III A and numerical results based on a full stochastic simulation of the Langevin equations follow in Sec. III B. Some concluding remarks are made in Sec. IV. Finally, an analysis of the moment equations for periodic solutions is contained in the Appendix.

II. THEORY

The stochastic differential equations defining the model are the fluctuating convective-diffusion equation for the colloidal number density, $N(\mathbf{x},t)$, and the fluctuating Navier-Stokes equation for the local fluid velocity field, $\mathbf{v}(\mathbf{x},t)$. The latter equation contains a nonlinear, nonlocal term involving the colloid number density, called active mixing, that is not present in traditional hydrodynamics, and is responsible for all the new phenomena. It is important to realize that this new term is by no means *ad hoc*. It results from the requirement of detailed balance [14,15] which insures the system relaxes to its proper equilibrium in the absence of external perturbations. Hence, the model is based on simple symmetries and has no adjustable parameters. For more details on the derivation of the model, and in particular, the origin of the active-mixing term, see, e.g., Refs. [16–22].

The equations of motion governing the evolution of the fields are

$$\frac{\partial N(\mathbf{x},t)}{\partial t}=D_0\nabla^2\mu(\mathbf{x},t)-\mathbf{v}(\mathbf{x},t)\cdot\nabla N(\mathbf{x},t)+\zeta(\mathbf{x},t) \quad (1)$$

and

$$\frac{\partial \mathbf{v}(\mathbf{x},t)}{\partial t}=\nu\nabla^2\mathbf{v}(\mathbf{x},t)-\mathbf{v}(\mathbf{x},t)\cdot\nabla\mathbf{v}(\mathbf{x},t)-\frac{\nabla p(\mathbf{x},t)}{\rho}+\frac{k_BT}{\rho n_c}\mu(\mathbf{x},t)\nabla N(\mathbf{x},t)+\mathbf{f}(\mathbf{x},t), \quad (2)$$

where

$$\mu(\mathbf{x},t)\equiv\int\frac{d\mathbf{k}}{(2\pi)^d}e^{-i\mathbf{k}\cdot\mathbf{x}}\frac{N(\mathbf{k},t)}{S^{(eq)}(\mathbf{k})}, \tag{3}$$

and with the Gaussian noise distributions defined by the moments,

$$\langle\zeta(\mathbf{x},t)\rangle=0,\ \langle\mathbf{f}(\mathbf{x},t)\rangle=\mathbf{0}, \tag{4}$$

$$\langle\zeta(\mathbf{x},t)\zeta(\mathbf{x}',t')\rangle=2D_0n_c(-\nabla^2)\delta(\mathbf{x}-\mathbf{x}')\delta(t-t'), \tag{5a}$$

and

$$\langle f_i(\mathbf{x},t)f_j(\mathbf{x}',t')\rangle$$

$$=2k_BT(\nu/\rho)[-\nabla^2\delta_{ij}-\nabla_i\nabla_j(\tfrac{1}{3}+\gamma)]\times\delta(\mathbf{x}-\mathbf{x}')\delta(t-t'), \tag{5b}$$

where n_c is the number density of colloidal particles, ρ is the fluid density, D_0 is the diffusion constant of the suspensions in the solvent, ν is the kinematic viscosity ($\nu\equiv\eta/\rho$, where η is the dynamic viscosity), p is the local pressure, and γ is the ratio of the bulk viscosity to the shear viscosity. The definition of $\mu(\mathbf{x},t)$ follows from de Gennes' expression for a generalized diffusion operator [23], as in Ref. [24]. The mass density of the colloidal particles is assumed to be equal to that of the solvent and both are taken to be incompressible, leading to the following relations:

$$\rho=\text{const},\quad\text{and}\ \nabla\cdot\mathbf{v}(\mathbf{x},t)=0. \tag{6}$$

This condition can be used to eliminate longitudinal terms such as the pressure gradient term in Eq. (2) and the term in $\nabla_i\nabla_j$ in the velocity noise correlation, Eq. (5b), which includes the bulk viscosity. As input to the model, the equilibrium structure factor must be specified. For this purpose, the three-dimensional hard-sphere structure factor in the Percus-Yevick approximation is used.

At this point, it is useful to note that Eqs. (1) and (2) do not evolve on the same time scale. This is easily seen if one looks at the ratio of the diffusion constants $P_t=\nu/D_0$, which is typically of the order of 10^6. (P_t stands for the Prandtl number, in analogy with thermal diffusion in fluids, and is sometimes referred to as the Schmidt number S_c). This means that as far as the relaxation of colloidal number-density fluctuations are concerned, the relaxation of velocity fluctuations is essentially instantaneous. This can be exploited to eliminate the velocity field and thus obtain a single nonlinear equation for the number-density field. It will sometimes be convenient to rescale the units and fields as follows: space is in units of σ, time is in units of σ^2/D_0, the number density, $N(\mathbf{r},t)$, is in units of n_c, and the velocity is in units of D_0/σ, with σ the particles' diameter. In these rescaled units, the infinite Prandtl number limit (also called the high friction limit) of Eqs. (1) and (2) together with Eq. (6), takes the following form in Fourier space:

$$\frac{\partial N(\mathbf{k},t)}{\partial t}=-\frac{k^2}{S^{(eq)}(k)}N(\mathbf{k},t)+2\alpha k_y\frac{\partial}{\partial k_x}N(\mathbf{k},t)+\xi(\mathbf{k},t)-\int\frac{d\mathbf{k}_1}{(2\pi)^d}\frac{N(\mathbf{k}-\mathbf{k}_1,t)}{k_1^2}\Bigg[\mathbf{j}_t(\mathbf{k}_1,t)\cdot(-i\mathbf{k})+\beta n_c\sigma^d\int\frac{d\mathbf{k}_2}{(2\pi)^d}\mathbf{k}\cdot\overleftrightarrow{\Phi}_{\mathbf{k}_1}\cdot\mathbf{k}_2N(\mathbf{k}_1-\mathbf{k}_2,t)\times\frac{N(\mathbf{k}_2,t)}{S^{(eq)}(k_2)}\Bigg], \tag{7}$$

where $(\overleftrightarrow{\mathbf{\Phi}}_{\mathbf{k}})_{ij}\equiv\delta_{ij}-\hat{\mathbf{k}}_i\hat{\mathbf{k}}_j$, $\beta\equiv(k_BT\sigma^{2-d})/(\eta D_0)$, d is the spatial dimension, and the dimensionless shear rate is given by $\alpha\equiv(\omega_0\sigma^2)/(2D_0)$. The rescaled random noise fields have the same type of distribution as before except for the value of the variance and the fact that $\mathbf{j}_t$ is now transverse. These changes appear only in the second moments, which are now rewritten, again in Fourier space, as

$$\langle\xi(\mathbf{k},t)\xi(\mathbf{k}',t')\rangle=\frac{2k^2}{n_c\sigma^d}(2\pi)^d\delta(\mathbf{k}+\mathbf{k}')\delta(t-t'), \tag{8a}$$

and

$$\langle\mathbf{j}_t(\mathbf{k},t)\mathbf{j}_t(\mathbf{k}',t')\rangle=2\beta k^2\overleftrightarrow{\mathbf{\Phi}}_{\mathbf{k}}(2\pi)^d\delta(\mathbf{k}+\mathbf{k}')\delta(t-t'). \tag{8b}$$

In three dimensions, the Stokes-Einstein relation gives $(k_BT)/(D_0\eta)=3\pi\sigma$, which leads to $\beta n_c\sigma^d=18\phi$, where $\phi=(\pi/6)n_c\sigma^3$, is the three-dimensional packing fraction. In two dimensions, the Stokes-Einstein relation does not hold because the drag coefficient depends logarithmically on a colloidal particle's velocity, cf. [25]. Nonetheless, this velocity dependence is weak (logarithmic) and for what follows we let $(k_BT)/(D_0\eta)=4\pi/\{1/2-\gamma-\ln[u\sigma/(8\nu)]\}$, where u is the average velocity of the colloidal particles with respect to the solvent and γ is Euler's constant. As an order of magnitude, a reasonable estimate for u is $u\sim D_0/\sigma$, which leads to the two-dimensional relation, $(k_BT)/(D_0\eta)\sim4\pi/[(1/2)-\gamma+\ln(8P_t)]$, where $P_t=\nu/D_0$ is the Prandtl number. Large variations of the Prandtl number, e.g., from $P_t=10^3$ to $P_t=10^{10}$ (which more than encompasses the typical range in values), lead to modest changes in the value of $(k_BT)/(D_0\eta)$, namely, from roughly $\pi/2$ to $\pi/6$, respectively. The value $(k_BT)/(D_0\eta)\sim\pi/4$ was arbitrarily chosen for our numerical work, and, as a result, in two dimensions, $\beta n_c\sigma^d\sim(\pi/4)n_c\sigma^2=\phi$, ϕ being the two-dimensional packing fraction. Finally, note that the nonlinear terms in the Langevin equations renormalize the bare diffusion constants, and hence, strictly speaking, the preceding discussion applies to the renormalized diffusion constant cf. Sec. II B.

A. Perturbative calculation

The main motivation for this work is our previous perturbative analysis of Eqs. (1)–(6), cf. Ref. [13]. There, we used the statistical field theory model presented above, and derived, to first order in perturbation theory, the nonequilibrium correction to the two-point correlation function, result-

ing from an applied linear shear gradient given by $\mathbf{v}_0 = \omega_0 x \hat{\mathbf{y}}$. The steady-state two-point correlation function is related to the structure factor by

$$\langle N(\mathbf{k})N(\mathbf{k}')\rangle = \int \frac{d\Omega}{2\pi}\int \frac{d\Omega'}{2\pi}\langle N(\mathbf{k},\Omega)N(\mathbf{k}',\Omega')\rangle = (2\pi)^d \delta(\mathbf{k}+\mathbf{k}')n_c S(k). \tag{9}$$

We thus obtained an expression for the first-order correction to the nonequilibrium structure factor. We focused on the shear gradient direction x as linear theory was argued to be a good approximation in the flow direction y (which is confirmed by the stochastic simulations of the present work). Letting q be the wave number in the rescaled units ($q = k_x\sigma$), the nonequilibrium structure was found to have the form

$$S(q) = \frac{1}{1 - n_c[c(q) + f(q) + f(-q)]}, \tag{10}$$

where $c(q)$ is the equilibrium direct correlation function in Fourier space. Using as input the equilibrium structure factor for a hard sphere system in the Percus-Yevick approximation, it was found that the first-order nonequilibrium correction $f(q)$ is given by the expression below:

$$n_c f(q) = \frac{3}{8\pi^2}\int_{y>0} d\mathbf{x}\frac{y^2+z^2}{[(x+q)^2+y^2+z^2]^2} \times \int_0^\infty dp\,\frac{\partial}{\partial p}\left(\frac{S^{(eq)}[\sqrt{(x+p)^2+y^2+z^2}]}{S^{(eq)}(|\mathbf{x}|)}\right) \times \exp\left[-\frac{1}{\alpha y}\int_0^p dr \frac{[(x+r)^2+y^2+z^2]}{S^{(eq)}[\sqrt{(x+r)^2+y^2+z^2}]}\right]. \tag{11}$$

This allowed us to construct an approximate phase diagram in the packing fraction-shear rate plane, with an instability line defined by the spinodal line $1/S(q^*)|_{\alpha=\alpha_{cr}} = 0$, where q^* is the position of the largest peak. This constituted one of the first theoretical predictions of a nonequilibrium transition to a lamellar pattern resulting from an applied shear in colloidal suspensions. In addition, our model includes a kind of hydrodynamic interaction induced by the active-mixing terms (see below), and is responsible for the instability; as far as we know, with the exception of some studies of models describing the more complicated effect of shear on polymers [26,27], these interactions were absent in the earlier works that offer strongest theoretical support for a transition to a layered state under shear, i.e., the numerical simulations [2–7]. It was thus imperative that the model equations be tested in a nonperturbative fashion to find out whether the instability in question was an artifact of the perturbative method, or indeed exists. The stochastic simulations described below confirm the existence of the instability.

In [13], an attempt was also made at determining, along with the instability line, a line representing the point where the system turns around from shear thinning to shear thickening. Since the viscosity may be written as an integral of $[S(q)-1]$, times other shear independent factors, we associated the transition from shear thinning to shear thickening to the point where the main peak of the structure factor stops decreasing and starts increasing, i.e., the point where $\partial S(q^*)/(\partial\alpha) = 0$. This point, however, is beyond the scope of this work, as viscosity calculations, while conceptually simple, are difficult to do numerically [28] and are not performed here.

The nonequilibrium correction was studied in various limits. For example, at zero wave number ($q=0$) and for small shear ($\alpha<1$), Eq. (11) reduces to

$$n_c f(0) = \frac{3}{8\pi^2}\alpha^{3/2}\frac{n_c \partial^2 c(q)/\partial q^2|_{q=0}}{[1-n_c c(0)]^{5/2}}C, \tag{12}$$

where $C = 1.848$ is a universal constant. Consequently, for long wavelengths the structure factor (and quantities with simple relations to the long wavelength parts of the structure factor) is expected to grow as $\alpha^{3/2}$ for small shear rates. For wave numbers in the range $q > \alpha^{1/2}$, the behavior crosses over to an α^2 dependence for small shear rates. The corresponding expression can be found in [13], [Eq. (28)].

In the opposite limit of infinite shear, Eq. (11) becomes even in y and simplifies to give

$$n_c f_\infty(q) = -\frac{3}{8\pi^2}\int d\mathbf{x}\frac{y^2+z^2}{[(x+q)^2+y^2+z^2]^2} n_c c(|\mathbf{x}|), \tag{13}$$

where now $f_\infty(q)$ is defined without the restriction that $y > 0$ in the integration. Hence, we can rewrite the infinite shear structure factor as

$$S_\infty(q) = \frac{1}{1 - n_c[c(q) + f_\infty(q)]}. \tag{14}$$

From this simplified expression, one easily determines a critical packing fraction ϕ_{cr}, below which no instability arises even for infinite shear rate. For the hard sphere model considered, that packing fraction was found to be 37.5% in three dimensions.

More generally, the behavior of the system, as suggested by the structure factor is one of monotonically increasing disorder in the flow direction (y), with increasing shear, but a more complex behavior in the shear gradient direction (x). In that direction, in Fourier space, the structure factor also flattens out for most wavelengths, except in the neighborhood of the main peak, where the structure factor initially decreases, but then increases, and eventually diverges at some large value of the shear rate when the packing fraction is greater than the critical packing fraction ϕ_{cr}, mentioned above.

As will be seen below, many of those predictions will be verified in the present work. However, the prediction that the

wavelength of the instability increases slightly with the packing fraction of the system turns out to be wrong as far as the two-dimensional stochastic simulations are concerned.

B. Moment equations

To further clarify the mechanisms at work in the creation and stabilization of the layered states under shear, we now examine approximate equations describing the evolution of the first and second colloid density moments. These two quantities characterize the essential physics; the first moment tracks the emergence of order in the system, and the second describes the evolution of fluctuations as the layers develop and stabilize. Dynamical equations for the moments were derived from the Fokker-Planck equation corresponding to the model equations in the limit of infinite Prandtl number (or high friction), cf. Eq. (7). In the original (nonrescaled) units, the Stratonovich form of the Fokker-Planck equation is

$$\frac{\partial P([N],t)}{\partial t} = -\int d\mathbf{k} \frac{\delta}{\delta N(\mathbf{k})} \Bigg[-D_0 \frac{k^2 N(\mathbf{k})}{S^{(eq)}(k)} + \omega_0 k_y \frac{\partial N(\mathbf{k})}{\partial k_x} - D_0 n_c k^2 (2\pi)^d \frac{\delta}{\delta N(-\mathbf{k})} - \frac{k_B T}{\eta} \int \frac{d\mathbf{k}_1}{(2\pi)^d} \int \frac{d\mathbf{k}_2}{(2\pi)^d} \frac{\mathbf{k}\cdot\overleftrightarrow{\Phi}_{\mathbf{k}_1}\cdot\mathbf{k}_2}{k_1^2} \times N(\mathbf{k}-\mathbf{k}_1) \left(\frac{N(\mathbf{k}_2)}{n_c S^{(eq)}(k_2)} + (2\pi)^d \frac{\delta}{\delta N(-\mathbf{k}_2)} \right) \times N(\mathbf{k}_1-\mathbf{k}_2) \Bigg] P([N],t). \quad (15)$$

Again we emphasize the need for the active-mixing term appearing in the above equation. It enables the system to relax to equilibrium, as can be seen by replacing the distribution $P([N],t)$ by the equilibrium distribution given by

$$P^{(eq)}([N],t) \propto \exp\left(-\frac{1}{2} \int \frac{d\mathbf{k}}{(2\pi)^d} \frac{N(\mathbf{k})N(-\mathbf{k})}{n_c S^{(eq)}(k)} \right), \quad (16)$$

and seeing that we indeed get $[\partial P^{(eq)}([N],t)/\partial t] = 0$. Equation (15) clearly shows the physical origin of the active-mixing term. Just as the random fluctuations in the number density (third term on the right-hand side) are balanced by the diffusion term, (first term on the right-hand side), the random fluctuations in the fluid velocities (fifth term on the right-hand side) which couple to ∇N in Eq. (1), are compensated by the active-mixing term (fourth term on the right-hand side).

A hierarchy of equations governing the nonequilibrium equal time moments of the distribution can easily be obtained from Eq. (15); for example, the first two moments obey

$$\frac{\partial \langle N(\mathbf{k}) \rangle}{\partial t} = \left(-\frac{D_0 k^2}{S^{(eq)}(k)} + \omega_0 k_y \frac{\partial}{\partial k_x} - \frac{k_B T}{\eta} \int \frac{d\mathbf{k}_1}{(2\pi)^d} \frac{\mathbf{k}\cdot\overleftrightarrow{\Phi}_{\mathbf{k}_1}\cdot\mathbf{k}}{k_1^2} \right) \langle N(\mathbf{k}) \rangle - \frac{k_B T}{\eta} \int \frac{d\mathbf{k}_1}{(2\pi)^d} \int \frac{d\mathbf{k}_2}{(2\pi)^d} \frac{\mathbf{k}\cdot\overleftrightarrow{\Phi}_{\mathbf{k}_1}\cdot\mathbf{k}_2}{k_1^2} \times \frac{\langle N(\mathbf{k}-\mathbf{k}_1) N(\mathbf{k}_1-\mathbf{k}_2) N(\mathbf{k}_2) \rangle}{n_c S^{(eq)}(k_2)} \quad (17)$$

and

$$\frac{\partial \langle N(\mathbf{k}) N(\mathbf{k}') \rangle}{\partial t} = \Bigg\{ \left[-\frac{D_0 k^2}{S^{(eq)}(k)} + \omega_0 k_y \frac{\partial}{\partial k_x} - \frac{k_B T}{\eta} \int \frac{d\mathbf{k}_1}{(2\pi)^d} \frac{\mathbf{k}\mathbf{k}:\overleftrightarrow{\Phi}_{\mathbf{k}_1}}{k_1^2} \right] \langle N(\mathbf{k}) N(\mathbf{k}') \rangle - \frac{k_B T}{\eta} \int \frac{d\mathbf{k}_1}{(2\pi)^d} \frac{\mathbf{k}\mathbf{k}':\overleftrightarrow{\Phi}_{\mathbf{k}_1}}{k_1^2} \times \langle N(\mathbf{k}-\mathbf{k}_1) N(\mathbf{k}'+\mathbf{k}_1) \rangle - \frac{k_B T}{\eta} \int \frac{d\mathbf{k}_1\, d\mathbf{k}_2}{(2\pi)^{2d}} \frac{\mathbf{k}\mathbf{k}_2:\overleftrightarrow{\Phi}_{\mathbf{k}_1} \langle N(\mathbf{k}-\mathbf{k}_1) N(\mathbf{k}_1-\mathbf{k}_2) N(\mathbf{k}_2) N(\mathbf{k}') \rangle}{\mathbf{k}_1^2 \quad n_c S^{(eq)}(k_2)} \Bigg\} + \{\mathbf{k} \leftrightarrow \mathbf{k}'\} + 2 D_0 n_c k^2 (2\pi)^d \delta(\mathbf{k}+\mathbf{k}'), \quad (18)$$

where $\{\mathbf{k}\leftrightarrow\mathbf{k}'\}$ denotes the preceding terms in curly brackets with $\mathbf{k}$ and $\mathbf{k}'$ interchanged.

In the homogeneous phase, i.e., for shears below any transition to the lamellar phase, an approximate equation for the sheared structure factor can be obtained by assuming a Gaussian form for the nonequilibrium distribution function (with, for now, zero mean) and introducing the structure factor, cf. Eq. (9); with this, Eq. (17) is trivial, and Eq. (18) becomes

$$\frac{\partial S(\mathbf{k})}{\partial t}=\left(-\frac{2D_0k^2}{S^{(eq)}(k)}+\omega_0k_y\frac{\partial}{\partial k_x}\right)S(\mathbf{k})+2D_0k^2 - \frac{2k_BT}{\eta}S(\mathbf{k})\int\frac{d\mathbf{k}_1}{(2\pi)^d}\frac{\mathbf{k}\cdot\vec{\mathbf{\Phi}}_{\mathbf{k}_1}\cdot\mathbf{k}}{k_1^2} \times\left[S(\mathbf{k}-\mathbf{k}_1)\left(\frac{1}{S^{(eq)}(k)}-\frac{1}{S^{(eq)}(|\mathbf{k}_1-\mathbf{k}|)}\right)+1\right] + \frac{2k_BT}{\eta}\int\frac{d\mathbf{k}_1}{(2\pi)^d}\frac{\mathbf{k}\cdot\vec{\mathbf{\Phi}}_{\mathbf{k}_1}\cdot\mathbf{k}}{k_1^2}S(\mathbf{k}-\mathbf{k}_1), \tag{19}$$

in which the symmetry $S(\mathbf{k})=S(-\mathbf{k})$ was used.

The integrals in this expression have UV divergences (in the limit of infinite cutoff) that are the usual ones associated with mode-coupling theories of the diffusion coefficient, cf. Ref. [29]. For example, in mode-coupling theory it is well known that the zero-frequency, one-loop, equilibrium collective diffusion constant is

$$D_C^{(eq)}(k)=\frac{D_0}{S^{(eq)}(k)}+\frac{k_BT}{\rho}\int\frac{d\mathbf{k}_1}{(2\pi)^d} \times\frac{\hat{\mathbf{k}}\cdot\vec{\mathbf{\Phi}}\_\mathbf{k}_1\cdot\hat{\mathbf{k}}}{D_C^{(eq)}(|\mathbf{k}-\mathbf{k}_1|)|\mathbf{k}-\mathbf{k}_1|^2+\nu k_1^2} \times\frac{S^{(eq)}(|\mathbf{k}-\mathbf{k}_1|)}{S^{(eq)}(k)}. \tag{20}$$

Since the boundary conditions on the surface of the colloidal particles are not explicitly included in mode-coupling theories, their effects appear in the form of the short-wavelength divergences if the UV cutoffs are set to infinity. This sensitivity to the short-wavelength details should be expected since the form of the Stokes-Einstein relation for the self-diffusion constant depends on the nature of the boundary condition used for the fluid motion at a colloidal particle's surface; for example, in three dimensions,

$$D_{SE}=\frac{k_BT}{\xi\pi\eta\sigma}, \tag{21}$$

where ξ is 3 for stick boundary conditions, 2 for slip, and 5/2 at the surface of a bubble. Note however, that whatever the boundary condition, the basic scaling properties of the Stokes-Einstein relation are the same, and, moreover, only involve single-colloid particle properties (for example, the colloid density or colloid-colloid structure factor do not appear). The scaling of the diffusion constant with particle size is also recovered in mode-coupling theory if the UV cutoff is proportional to σ^{-1}, cf. Ref. [29].

All the UV divergences in both Eqs. (19) and (20) have the same origin, and are fixed by replacing the bare diffusion constant, D_0, by the finite, physical diffusion constant D_{SE}, and an explicitly infinite (actually strongly cutoff-dependent) part that cancels the UV divergences. To one loop order, the correction to the self-diffusion constant is

$$D_0=D_{SE}-\frac{k_BT}{\eta}\int\frac{d\mathbf{k}_1}{(2\pi)^d}\frac{\hat{\mathbf{k}}\cdot\vec{\mathbf{\Phi}}_{\mathbf{k}_1}\cdot\hat{\mathbf{k}}}{k_1^2}, \tag{22}$$

which is identical to the form derived by Keyes and Oppenheim [29] in their analysis of the Stokes-Einstein expression in mode-coupling theory and which results in the usual scaling properties given in Eq. (21).

Since the packing fractions required to get an instability are high, the use of the Stokes-Einstein relation may be questioned. However, theoretical work by Beenakker [30], experimental work by Kops-Werkhoven and Fijnaut [31], and van Blaaderen *et al.* [32], as well as Brownian dynamics simulations by Rastogi, Wagner, and Lustig [7], suggest that the Stokes-Einstein relation between the diffusion coefficient of the colloidal particles and the fluid viscosity remains a good approximation at high packing fractions, at least for a system of hard spheres. And although it is of little relevance to our model, it is interesting to note that the Brownian dynamics simulations of Rastogi, Wagner, and Lustig [7], lead to the conclusion that the Stokes-Einstein relation may even be extended to the nonequilibrium case in the presence of shear, up until a lamellar phase forms. At that point, the Stokes-Einstein relation breaks down, which probably means that the self-diffusion coefficient is no longer simply related to the collective diffusion constant since long-range order is now present. These simulations also show that the instability that arises is independent of the system size.

In the Introduction we mentioned that our calculation includes a kind of hydrodynamic interaction. This should be apparent from the preceding equations, all of which contain the Oseen tensor $\vec{\mathbf{\Phi}}_{\mathbf{k}}/k^2$. Nonetheless, the connection between the mode-coupling approach and the usual ones that study hydrodynamic interactions in suspensions, cf. Refs. [33–35], is less obvious. To see how they compare, we use Eq. (22) in (20) to show that

$$D_C^{(eq)}(k)=\frac{D_{SE}}{S^{(eq)}(k)}+\frac{k_BT}{\eta} \times\int\frac{d\mathbf{k}_1}{(2\pi)^d}\frac{\hat{\mathbf{k}}\cdot\vec{\mathbf{\Phi}}_{\mathbf{k}_1}\cdot\hat{\mathbf{k}}}{k_1^2}\frac{S^{(eq)}(|\mathbf{k}-\mathbf{k}_1|)-1}{S^{(eq)}(k)} \tag{23}$$

in the infinite Prandtl number limit. To first order in density, Eq. (23) reduces to the expression obtained by Altenberger and Deutch, cf. Ref. [35]. For example, using the Percus-Yevick hard sphere structure factor, this gives $D_C^{(eq)}(k=0)/D_{SE}\sim 1+2\phi$; Batchelor's calculation [34], gives $D_C^{(eq)}(k=0)/D_{SE}\sim 1+1.45\phi$. Finally, we note that the

active-mixing induced hydrodynamic interactions arise from the interaction potentials between the colloidal particles, and in particular will be present in ultradilute, poorly screened suspensions of charged colloids. While these systems exhibit strong interparticle correlations, the traditional corrections due to hydrodynamic interactions are negligible; nonetheless, significant corrections to the diffusion constant will arise from Eq. (23).

If we now rewrite Eq. (19), eliminating D_0 in favor of D_{SE} using Eq. (22), in the limit of infinite Prandtl number $P_t \to \infty$, we find that

$$\frac{\partial S(\mathbf{k})}{\partial t} = \left(-\frac{2D_{SE}k^2}{S^{(eq)}(k)} + \omega_0 k_y \frac{\partial}{\partial k_x} \right) S(\mathbf{k}) + 2D_{SE}k^2 - \frac{2k_BT}{\eta} S(\mathbf{k}) \int \frac{d\mathbf{k}_1}{(2\pi)^d} \frac{\mathbf{k}\cdot\overleftrightarrow{\Phi}_{\mathbf{k}_1}\cdot\mathbf{k}}{k_1^2} \times \left[S(\mathbf{k}-\mathbf{k}_1) \left(\frac{1}{S^{(eq)}(k)} - \frac{1}{S^{(eq)}(|\mathbf{k}_1-\mathbf{k}|)} \right) + 1 - \frac{1}{S^{(eq)}(k)} \right] + \frac{2k_BT}{\eta} \times \int \frac{d\mathbf{k}_1}{(2\pi)^d} \frac{\mathbf{k}\cdot\overleftrightarrow{\Phi}_{\mathbf{k}_1}\cdot\mathbf{k}}{k_1^2} [S(\mathbf{k}-\mathbf{k}_1)-1]. \tag{24}$$

Equation (24) is now free of UV divergences. However, there will be IR divergences for $d \leqslant 2$ as long as $S(\mathbf{k}) \neq S^{(eq)}(k)$; this divergence arises from the well-known long-time tail problem in two dimensions, cf. Eq. (20), which makes $D_{SE} \propto \ln(k)$ as $k \to 0$. Note that since the phenomena we are concerned with here occur at *nonzero* wave vectors, the logarithmic divergence is not numerically significant for the wave vectors on the two-dimensional lattices used below.

To make contact with the linear theory of Ronis [24] it is instructive to rewrite Eq. (24) as

$$\frac{\partial S(\mathbf{k},t)}{\partial t} = \omega_0 k_y \frac{\partial S(\mathbf{k},t)}{\partial k_x} - 2\Gamma(\mathbf{k},t) S(\mathbf{k},t) + 2\mathcal{N}(\mathbf{k},t), \tag{25}$$

where the effective nonequilibrium relaxation rate and noise strength are given by

$$\Gamma(\mathbf{k},t) \equiv \frac{D_{SE}k^2}{S^{(eq)}(k)} + \frac{k_BT}{\eta} \int \frac{d\mathbf{k}_1}{(2\pi)^d} \frac{\mathbf{k}\cdot\overleftrightarrow{\Phi}_{\mathbf{k}_1}\cdot\mathbf{k}}{k_1^2} \times \left[S(\mathbf{k}-\mathbf{k}_1,t) \left(\frac{1}{S^{(eq)}(k)} - \frac{1}{S^{(eq)}(|\mathbf{k}_1-\mathbf{k}|)} \right) + 1 - \frac{1}{S^{(eq)}(k)} \right], \tag{26}$$

and

$$\mathcal{N}(\mathbf{k},t) \equiv D_{SE}k^2 + \frac{k_BT}{\eta} \int \frac{d\mathbf{k}_1}{(2\pi)^d} \frac{\mathbf{k}\cdot\overleftrightarrow{\Phi}_{\mathbf{k}_1}\cdot\mathbf{k}}{k_1^2} [S(\mathbf{k}-\mathbf{k}_1,t)-1], \tag{27}$$

respectively.

In the steady state, $[\partial S(\mathbf{k},t)/\partial t] = 0$, and the formal solution to Eq. (25) is

$$S(\mathbf{k}) = \int_{k_x}^{\infty} \frac{dk_x'}{\omega_0 k_y} \exp\left(-2 \int_{k_x}^{k_x'} \frac{dk_x''}{\omega_0 k_y} \Gamma(\mathbf{k}'') \right) 2\mathcal{N}(\mathbf{k}') \quad \text{for } \omega_0 k_y > 0, \tag{28a}$$

$$= \int_{-\infty}^{k_x} \frac{dk_x'}{\omega_0 k_y} \exp\left(2 \int_{k_x'}^{k_x} \frac{dk_x''}{\omega_0 k_y} \Gamma(\mathbf{k}'') \right) 2\mathcal{N}(\mathbf{k}') \quad \text{for } \omega_0 k_y < 0, \tag{28b}$$

where $\mathbf{k}'$ has its k_x component replaced by k_x', etc. Note that Eqs. (28a) and (28b) imply that $S(\mathbf{k}) = S(-\mathbf{k})$. Also notice the formal similarity between Eq. (28) and the result for the linear theory of Ronis, although here $\mathcal{N}$ and Γ depend on S. Nonetheless, Eq. (28) is a good starting point for numerical work (see below). Finally, in the plane perpendicular to the flow direction, $\omega_0 k_y = 0$, the steady-state solution to Eq. (25) takes the form

$$S(k_x) = \frac{\mathcal{N}(k_x)}{\Gamma(k_x)}. \tag{29}$$

As mentioned in the previous section, simulations confirm that for large shear rates, $S(\mathbf{k}) \sim 1$ as long as $(\omega_0 \sigma^3 k_y)/D_{SE} \gg 1$. Substituting $S(\mathbf{k}-\mathbf{k}_1,t)$ by 1 in the integrand of Eqs. (26) and (27) should thus be a good approximation to the infinite shear expression for $S(k_x)$, and, not surprisingly, leads to the same expression for the infinite shear structure factor as that obtained in the one-loop calculation of Morin and Ronis, cf. Eq. (14), namely,

$$S(k_x) = \frac{1}{1 - n_c(c(k_x) + f(k_x))}, \tag{30}$$

where

$$f(k_x) = -\frac{k_BT}{D_{SE}\eta} \int \frac{d\mathbf{k}_1}{(2\pi)^d} \frac{\hat{\mathbf{k}}\cdot\overleftrightarrow{\Phi}_{\mathbf{k}_1}\cdot\hat{\mathbf{k}}}{k_1^2} c(\mathbf{k}-\mathbf{k}_1), \tag{31}$$

$c(k)$ being the equilibrium direct correlation function related to the structure factor as $S^{(eq)}(k) = 1/[1 - n_c c(k)]$. Note that for finite shear, Eq. (29) reduces to the one-loop expression given in [13] when the expression obtained in the linear theory (zero-loop) is used for $S(\mathbf{k})$ in Eqs. (26) and (27), and the nonequilibrium terms are all put into the numerator.

According to the analysis of the preceding section and [13], suspensions that are spatially uniform on average are unstable for shear rates beyond some critical value, and in the Gaussian approximation it is straightforward to extend the analysis to include this case, thereby allowing nonzero $\langle N(\mathbf{k}) \rangle$. We first split the number density field into two distinct parts by writing

$$N(\mathbf{k}) \equiv \langle N(\mathbf{k}) \rangle + \delta N(\mathbf{k}),$$

where $\langle N(\mathbf{k}) \rangle$, when nonzero, characterizes the long-range order at wave number $\mathbf{k}$, and $\delta N(\mathbf{k})$, gives the fluctuations around the average. Hence,

$$\begin{aligned} \langle N(\mathbf{k}) N(\mathbf{k}') \rangle &= \langle N(\mathbf{k}) \rangle \langle N(\mathbf{k}') \rangle + \langle \delta N(\mathbf{k}) \delta N(\mathbf{k}') \rangle \\ &\equiv \langle N(\mathbf{k}) \rangle \langle N(\mathbf{k}') \rangle + n_c s(\mathbf{k};\mathbf{k}'). \end{aligned} \tag{32}$$

Just as above, fluctuations are assumed to have a Gaussian distribution (now with nonzero mean). Here we further simplify matters by making the assumption that the variance is diagonal in wave vectors; i.e., we take $s(\mathbf{k};\mathbf{k}') \approx (2\pi)^d \delta(\mathbf{k}+\mathbf{k}') s(\mathbf{k})$. (More general equations for spatially periodic systems are presented in the Appendix.) With these two approximations, Eq. (17) becomes

$$\begin{aligned} \frac{\partial \langle N(\mathbf{k}) \rangle}{\partial t} = & \left[-\frac{D_{SE} k^2}{S^{(eq)}(k)} + \omega_0 k_y \frac{\partial}{\partial k_x} - \frac{k_B T}{\eta} \int \frac{d\mathbf{k}_1}{(2\pi)^d} \frac{\mathbf{k} \cdot \overleftrightarrow{\Phi}_{\mathbf{k}_1} \cdot \mathbf{k}}{k_1^2} \right. \\ & \left. \times \left(\frac{s(\mathbf{k}-\mathbf{k}_1)}{S^{(eq)}(k)} - \frac{1}{S^{(eq)}(k)} + 1 - \frac{s(\mathbf{k}-\mathbf{k}_1)}{S^{(eq)}(\mathbf{k}-\mathbf{k}_1)} \right) \right] \\ & \times \langle N(\mathbf{k}) \rangle - \frac{k_B T}{\eta} \int \frac{d\mathbf{k}_1}{(2\pi)^d} \int \frac{d\mathbf{k}_2}{(2\pi)^d} \frac{\mathbf{k} \cdot \overleftrightarrow{\Phi} \mathbf{k}_1 \cdot \mathbf{k}_2}{k_1^2} \\ & \times \langle N(\mathbf{k}-\mathbf{k}_1) \rangle \langle N(\mathbf{k}_1-\mathbf{k}_2) \rangle \frac{\langle N(\mathbf{k}_2) \rangle}{n_c S^{(eq)}(k_2)}. \end{aligned} \tag{33}$$

Finally, note that as in the analysis of the disordered state described above, the renormalized (physical) Stokes-Einstein diffusion constant D_{SE} was introduced in the previous equation instead of the bare self-diffusion constant D_0.

The full expression for the variance is considerably more complicated than Eq. (25), even within the Gaussian approximation. In order to simplify matters, we only present it under the assumption already used above; i.e., that fluctuations of interest are diagonal. This cannot be exact if $\langle N(\mathbf{k}) \rangle \neq 0$, and more general expressions for spatially periodic systems are presented in the Appendix.

After some straightforward algebra, it turns we obtain the same form as Eq. (24), with the modification that inside the various integrands we let $S(\mathbf{k}-\mathbf{k}_1) \to |\langle N(\mathbf{k}-\mathbf{k}_1) \rangle|^2/(n_c V) + s(\mathbf{k}-\mathbf{k}_1)$, where V is the volume of the system. Note that the volume factor arises from the relation between the two-point correlation function and the structure factor, cf. Eq. (9). In a finite system, the wave vectors are discrete and $(2\pi)^d \delta(\mathbf{k}+\mathbf{k}') \to V \delta_{\mathbf{k},-\mathbf{k}'}$. This modification to $S(\mathbf{k})$ inside the integrand perhaps should be expected since the total nonequilibrium density-density correlation function is the physically relevant quantity, and in fact is just $|\langle N(\mathbf{k}-\mathbf{k}_1) \rangle|^2/(n_c V) + s(\mathbf{k}-\mathbf{k}_1)$. Hence,

$$\begin{aligned} \frac{\partial s(\mathbf{k})}{\partial t} = & \left\{ -\frac{2 D_{SE} k^2}{S^{(eq)}(k)} + \omega_0 k_y \frac{\partial}{\partial k_x} \right. \\ & - \frac{2 k_B T}{\eta} \int \frac{d\mathbf{k}_1}{(2\pi)^d} \frac{\mathbf{k} \cdot \overleftrightarrow{\Phi}_{\mathbf{k}_1} \cdot \mathbf{k}}{k_1^2} \\ & \times \left[(s(\mathbf{k}-\mathbf{k}_1) + \left| \langle N(\mathbf{k}-\mathbf{k}_1) \rangle \right|^2/(n_c V)) \right. \\ & \times \left(\frac{1}{S^{(eq)}(k)} - \frac{1}{S^{(eq)}(|\mathbf{k}_1-\mathbf{k}|)} \right) \\ & \left. \left. + 1 - \frac{1}{S^{(eq)}(k)} \right] \right\} s(\mathbf{k}) \\ & + \frac{2 k_B T}{\eta} \int \frac{d\mathbf{k}_1}{(2\pi)^d} \frac{\mathbf{k} \cdot \overleftrightarrow{\Phi}_{\mathbf{k}_1} \cdot \mathbf{k}}{k_1^2} \\ & \times [s(\mathbf{k}-\mathbf{k}_1) + |\langle N(\mathbf{k}-\mathbf{k}_1) \rangle|^2/(n_c V) - 1] + 2 D_{SE} k^2, \end{aligned} \tag{34}$$

Apart from the shear term, the terms in the first two lines of the preceding equation are diffusionlike where the nonlinear parts [i.e., those with the integrand depending on $s(\mathbf{k})$ and $\langle N(\mathbf{k}) \rangle$] arise from active mixing. The last two lines include the usual additive noise for the number density fluctuations, and multiplicative noise caused by velocity fluctuations that couple through the convective term.

It is important to realize that Eq. (33) will not necessarily stabilize if a one-dimensional pattern develops since the projection operator will make the cubic $\langle N(\mathbf{k}) \rangle$ term in the equation (the nonlinear stabilizing term) zero. Hence, unless the nonlinear diffusion term stabilizes itself, Eq. (33) has unstable solutions. Higher-order corrections might cure this problem. In fact, the one-loop correction to the cubic term does indeed contain terms independent of the projection operator which could stabilize the system. However, we do not delve on such matters as this section is mostly intended to show that the instability can be understood in the usual manner of simple linear instability in the effective diffusion term.

III. RESULTS

The original analysis of the system of equations was done for a three-dimensional system. For this problem, however, three-dimensional stochastic simulations are prohibitively memory and CPU intensive for the sizes of grid and time-step that seem to be required for numerical stability. This forces our investigations to be carried out in two dimensions. Hence, this numerical work cannot be used as a quantitative comparison with the theoretical work of [13]. Instead, we will make a qualitative comparison with things like the prediction that the model equations have an instability to the formation of lamellae, which gives rise to a large peak in the structure factor, near the main peak of the equilibrium structure factor.

Even though the numerical work is done on a two-dimensional grid, the analytical three-dimensional Percus-

Yevick approximation to the equilibrium hard sphere structure factor was used for convenience. One important consequence of working in two dimensions is that higher packing fractions are required. This should be expected since, among other things, the close-pack limit is higher than in three dimensions. This can be seen more quantitatively by considering the packing fraction below which no lamellae can form, ϕ_{cr}, even at infinite shear. As was mentioned above, in three dimensions Eq. (14) leads to $\phi_{cr}=0.375$. In two dimensions Eq. (13) becomes

$$n_c f_\infty(q) = -\frac{1}{16\pi}\int d\mathbf{x}\frac{y^2}{[(x+q)^2+y^2]^2} n_c c(|\mathbf{x}|). \quad (35)$$

The above expression contains an infrared divergence and thus requires a lower limit cutoff similar to those seen in the mode-coupling theory of the diffusion constant in two dimensions, cf. Sec. II B. Since the calculations are performed on a relatively small finite system (albeit with periodic boundary conditions) we are not too concerned by this and introduce an IR cutoff in order to estimate the critical packing fraction. Based on the parameters used in the numerical simulations, the lower wave number limit is $k_{min}=0.245$, which leads to a critical packing fraction of $\phi_{cr}=0.558$. Furthermore, note that ϕ_{cr} increases with decreasing k_{min}, or equivalently with increasing volume, which implies that fluctuations prevent ordering in very large two dimensional systems. This however is irrelevant for our stochastic simulations since even with $k_{min}\sim 10^{-4}$, representing a system size of the order of 10^5–$10^6\sigma$, the critical packing fraction remains around 62%. Consequently, the concentrations of colloidal particles needed to get an instability in two dimensions are high and in the range where freezing is expected in three dimensions. Despite these drawbacks, we believe the two-dimensional stochastic simulations to be a good test of short- to intermediate-range aspects of the model under the application of a linear shear gradient.

A. Moment equations

The moment equations were solved numerically in two ways. In the first, the onset of the instability was examined by solving Eq. (28) iteratively on a grid. We used the current $S(\mathbf{k})$ to calculate $\mathcal{N}(\mathbf{k}')$ and $\Gamma(\mathbf{k}'')$ by fast-Fourier transforms; these were then used to recalculate the structure factor, the entire procedure being repeated until convergence was obtained. The task is further simplified by noting that Eq. (28a) implies that

$$S(\mathbf{k}-\Delta k_x\hat{\mathbf{e}}_1) = \exp\left(-2\int_{k_x-\Delta k_x}^{k_x}\frac{dk_x'}{\omega_0 k_y}\Gamma(\mathbf{k}')\right)S(\mathbf{k}) + 2\int_{k_x-\Delta k_x}^{k_x}\frac{dk_x'}{\omega_0 k_y} \times \exp\left(-2\int_{k_x-\Delta k_x}^{k_x'}\frac{dk_x''}{\omega_0 k_y}\Gamma(\mathbf{k}'')\right)\mathcal{N}(\mathbf{k}') \quad \text{for } \omega_0 k_y>0, \quad (36)$$

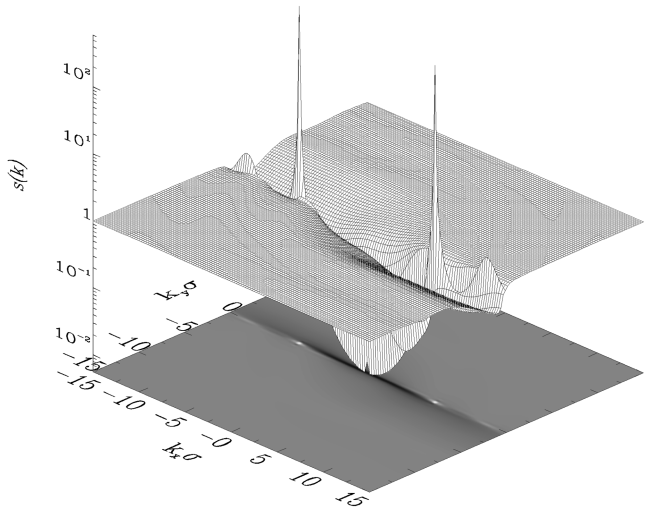

FIG. 1. Structure factor obtained from the moment equations in the homogeneous phase for a shear rate of $8400D_{SE}/\sigma^2$ [$\alpha \equiv \omega_0\sigma^2/(2D_{SE})=4250$] and $\phi=0.6$. The equilibrium packing fraction was 0.6 and a 243×161 grid with $-29.97\leqslant k_x\leqslant 29.97$ and $-19.82\leqslant k_y\leqslant 19.82$ (in units of σ^{-1}) was used. Note that an analysis of several runs shows that $S(k_{max})\sim|\omega_0-\omega_{cr}|^{-1.3}$, where $\omega_{cr}\approx 8780D_{SE}/\sigma^2$ ($\alpha=4390$) is the limit of stability point for this density.

with a similar expression for $\omega_0 k_y<0$; Eq. (29) is used for $k_y=0$. In this last expression, Δk_x is the lattice spacing in the k_x direction and $\hat{\mathbf{e}}_1$ is a unit vector along x, and all fields have the same values of k_y. The needed integrations were done by linearly interpolating $\mathcal{N}(\mathbf{k}')$ and $\Gamma(\mathbf{k}'')$ between the grid points, thereby resulting in expressions containing various error functions (the interpolation is necessary if expressions that are valid at small shear are to be obtained). Finally, the size of the grid was adjusted so that $S(\mathbf{k})\sim 1$ could be used in Eq. (36) outside the grid.

Figures 1 and 2 show some results of this calculation for

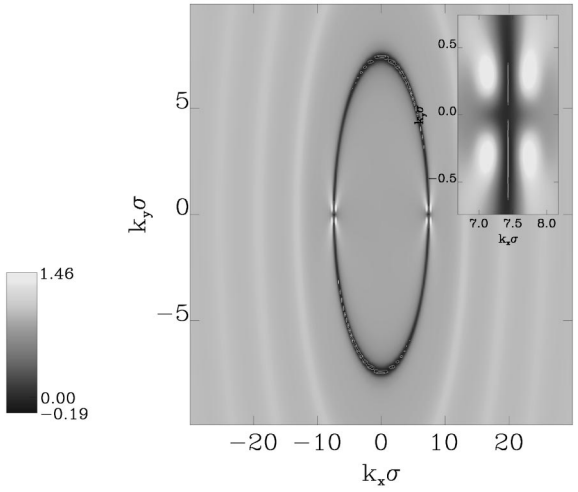

FIG. 2. The steady-state diffusion Onsager coefficient, $\Gamma(\mathbf{k},t)S^{(eq)}(k)/k^2$, cf. Eq. (26). The contours show where $\Gamma(\mathbf{k},t)=0$ with increasing shear. The system and numerical details are the same as in Fig. 1. The inset shows the behavior near a maximum of the structure factor, and in particular shows the quadrupolar pattern suggested by Eq. (A13).

a shear rate close to the instability. In Fig. 1 we see the characteristic distortion of the structure factor at high shear, although unlike the linear theories, now there are large changes in the structure factor for $k_y=0$. An interesting insight into the nature of the instability is obtained by considering effective Onsager diffusion coefficient, $\Gamma(k,t)S^{(eq)}(k)/k^2$, cf. Eq. (26), shown in Fig. 2. For sufficiently high shear, a pair thin crescent shaped regions where $\Gamma(k,t)<0$ appear. As the shear increases the negative region increases and approaches the $k_y=0$ line. The inset in Fig. 2 shows the quadrupolar symmetry expected near the peak maxima from the analysis of ordered periodic states given in the Appendix, cf. Eq. (A13).

The appearance of a region with $\Gamma(k,t)<0$ does not imply that the homogeneous state is unstable. For $k_y\neq 0$, the shear stretches fluctuations in the shear-gradient (x) direction, specifically, as $k_x\rightarrow k_x+\omega_0 k_y t$; hence, fluctuations with wave numbers initially in the unstable regime, will grow only until their wave numbers stretch to a point where they leave the region of negative Γ. Of course, the rate of stretching depends on k_y, and indeed the instability occurs when the negative Γ region reaches the k_x axis.

In a second approach, the coupled Eqs. (33) and (34) were simulated numerically on a rectangular grid. The lattice was chosen to have 243 grid points in the k_x direction with $-29.97\leqslant k_x\leqslant 29.97$ in units of $1/\sigma$, and 81 grid points in the k_y direction with $-9.91\leqslant k_y\leqslant 9.91$. A nonsquare lattice is used because in the flow direction (the y direction), the high shear structure factor goes to unity rapidly with increasing wave number, whereas the same is not true in the shear gradient direction (the x direction). In addition, reducing the wave number range in the y direction allows for more resolution at small wave numbers where interesting behavior may be found. The rescaled parameters described previously were used, together with a packing fraction of 60% and a shear rate of $\alpha=5000$. The same parameters will be used for the Langevin simulations.

The infinite Prandtl number limit moment equations were used, including terms arising from velocity noise fluctuations. The structure factor and Onsager diffusion coefficient for this case are shown in Figs. 3 and 4. The main results of this exercise are threefold. First, a sinusoidal pattern develops with a wave-vector corresponding to the position of the main peak of the equilibrium structure factor, apparently independent of the initial conditions. Specifically, two initial configurations were considered. One had $\langle N(\mathbf{k})\rangle$ small and random (as white noise) and $s(\mathbf{k})=S^{(eq)}(k)$. The other had $\langle N(\mathbf{x})\rangle$ set to $\sin(k_x' x)$ plus small fluctuations, where $k_x'\neq k_{max}$ (k_{max} is the position of the main peak of the equilibrium structure factor) and where the initial variance was set to $s(\mathbf{k})=1$ for $k_y\neq 0$ and $s(\mathbf{k})=S^{(eq)}(k)$ for $k_y=0$. Both cases led to the same steady state.

Secondly, within a few diffusion times, the nonlinear diffusion operators of both $\langle N(\mathbf{k})\rangle$ and $s(\mathbf{k})$ evolve from a configuration with a band of unstable modes, cf. Fig. 2, to a configuration where a single grid point in k space remains unstable, cf. Fig. 4. Note that the quadrupolar symmetry seen in the disordered phase is still very apparent. Furthermore, the value of the nonlinear diffusion operators at the unstable grid point is about -11 at one diffusion time and slowly increases thereafter. The relevance of this value will be discussed later in the light of the Langevin simulation results.

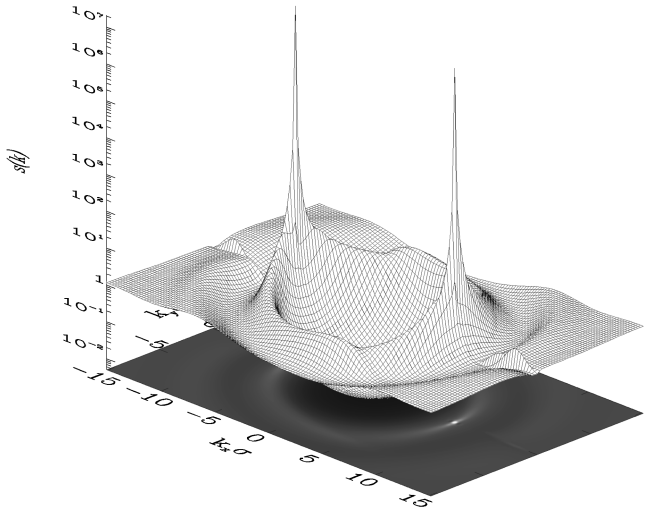

FIG. 3. The structure factor, $s(\mathbf{k})$, in the ordered phase at $t=0.3937D_0/\sigma^2$ when $\alpha=5000$.

Finally, we show the density-density correlation function, $s(\mathbf{k})$, cf. Eq. (32), in Fig. 3. Even on the diffusion time scale, the peaks have grown very large. Moreover, the algebraic tails or sidebands suggested by the analysis of spatially periodic states given in the Appendix, cf. Eq. (A14), are clearly visible and have the expected symmetry. The numerical data suggests that the sidebands diverge like $|\mathbf{k}-\mathbf{G}|^{-2.75\pm 0.25}$. This is reminiscent of the Goldstone mode sidebands in x-ray scattering from crystals and has important implications for the existence of true long-range order, especially in low spatial dimensions.

As stated earlier, however, the approximate method of moments outlined in this section has a main drawback in that the diffusion operators may never stabilize. The unstable modes shown above remain and lead to an ever increasing amplitude of the sinusoidal pattern. At least part of the problem is seen in Eq. (33) where the cubic $\langle N(\mathbf{k})\rangle$ term will vanish for a one-dimensional pattern because of the projection operator $\overleftrightarrow{\Phi}_{\mathbf{k}}$ appearing in the integrand. Higher-order corrections most probably cure this problem; one can easily

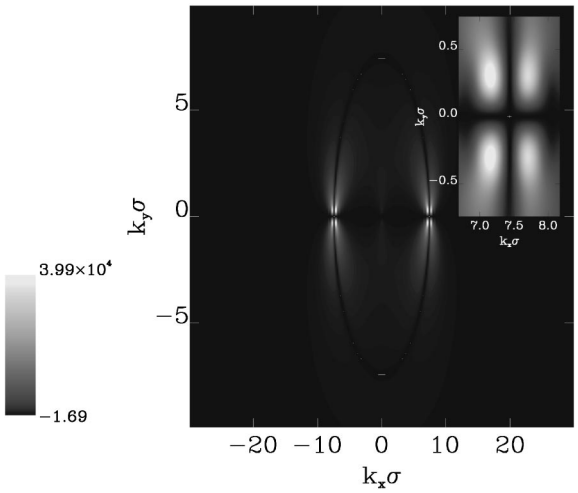

FIG. 4. The Onsager diffusion coefficient for the case shown in Fig. 3.

show that terms arise without the troublesome projection operator in higher-order perturbative treatments of the equations. Indeed, given how small the unstable regions are and how large and positive Γ becomes in the adjacent regions, cf. the inset of Fig. 4, it is quite reasonable that any mode coupling between these modes should lead to a stabilization of the pattern. Nonetheless, the higher-order corrections are quite complicated and are beyond the scope of this work.

The analysis of this section has allowed us to picture the instability to the formation of layers of colloidal particles flowing at different speeds as a more standard problem of linear instability. Numerical simulations of the coupled equations representing long-range order $\langle N(\mathbf{k})\rangle$, and short-range order $s(\mathbf{k})$ showed that there is a transient time where the growth rate of the layers is single exponential, and for which the wave number of the unstable mode corresponds to the position of the main peak of the structure factor, which is in disagreement with our previous predictions based on perturbation theory that the stripe pattern would form at a lower wave number than the peak position of the equilibrium structure factor.

B. Langevin equations

The high-friction limit of the model equations with random noise, Eq. (7), was simulated numerically on a two-dimensional grid of 128×128 points using a finite difference scheme for spatial derivatives and a stochastic Runge-Kutta algorithm due to Helfand [36,37] for the propagation in time. Although several more elaborate numerical schemes [38] were tried, Runge-Kutta gave the best results. For the purpose of the stochastic simulation, it was practical to use the rescaled units and fields described earlier.

In rescaled units, the time increment used in the stochastic simulations is $\Delta t=10^{-6}$ and the distance between neighboring lattice sites is $\Delta x=0.1$, to insure a sufficiently large wave-vector range (i.e., $-20<kx,ky<20$ in units of $1/\sigma$). The only input parameter left is the Prandtl number. Typical values are of the order of $P_t=10^6$, which proved to be impractical for numerical calculations as the Δt needed to insure stability of the velocity equations was much too small for the time scale of the number density equation. Hence, two limit cases were considered. First, a much smaller Prandtl number was used, namely, $P_t=10^3$, and second, the infinite Prandtl number equation, Eq. (7), was used.

The infinite Prandtl number equation also proved to be difficult to integrate numerically, and in order to use the stochastic Runge-Kutta algorithm, we have neglected the multiplicative velocity noise terms. A crude estimate shows that these terms are only important compared to the usual convective terms when $\alpha k_y \leqslant 2\beta k_{max}$, and are thus important only for very long wavelength fluctuations (in the velocity direction) at high shear rates.

Both of the methods just described gave comparable results and those presented were obtained from stochastic simulations of the infinite Prandtl number equations.

All runs were done at a packing fraction of 60%, which insures that the system becomes unstable at a finite shear rate (at least from estimate from a one-loop correction to mean-field theory), even in two dimensions. A sample run was performed, starting with a shear rate of $\alpha=1000$. When, after two to five diffusion times, no appreciable increase in the main peak of the structure factor was seen, the shear rate was increased, and the run continued. This was repeated a few times to make sure it was reproducible and independent of initial conditions. An appreciable increase in the main peak of the structure factor was seen after a few diffusion times once the shear rate was increased to $\alpha=4500$, although a clear striped phase was not seen within a few diffusion times. At $\alpha=5000$, the system is clearly unstable to the formation of stripes in colloid concentration, and we report on this case in detail below. Finally, note that while the critical value of α is comparable to that obtained from the moments analysis (where we find that $\alpha_{cr}=4760$ for the grid parameters used in the Langevin calculation) strictly speaking, the ratio of D_0/D_{SE} (which should be of order unity) must be known before a rigorous comparison can be made.

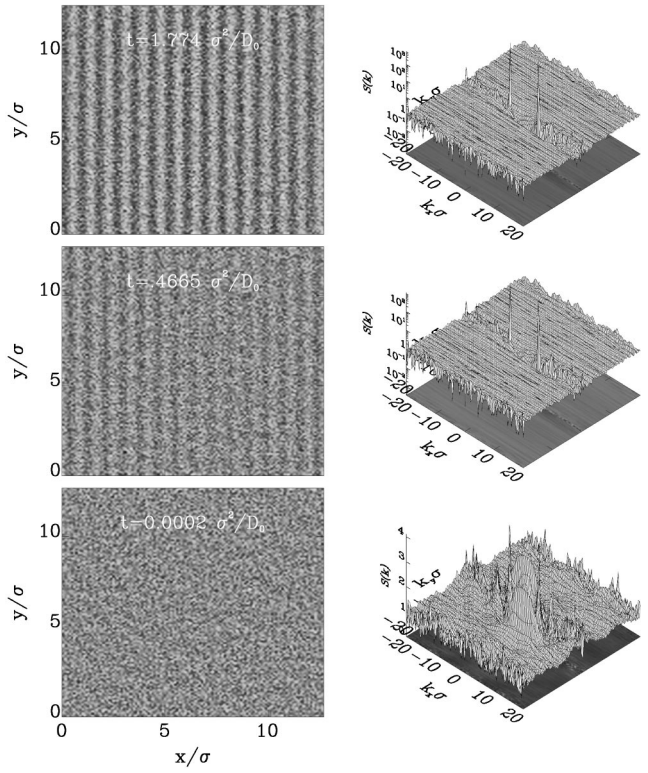

FIG. 5. Configurations $N(\mathbf{r})$ and $S(\mathbf{k})$ obtained by solving the Langevin equations. The system parameters are as in the preceding figures. The results are averaged over a small time window (500 time steps or 0.004 diffusion times at k_{max}).

The following results of the numerical simulation show various aspects of the evolution of a system, as described by our model equations, from a homogeneous state to a striped phase. Such a steady state is reached with a packing fraction of 60% and a shear rate of $\alpha=5000$. Figure 5 shows the configuration at various stages in the evolution of the main peak. At very early times, the structure factor already shows the effect of shear, although the number density still appears perfectly homogeneous. Very quickly, the structure factor takes the form depicted in the upper part of Fig. 5, i.e., $S(k_x,k_y)\sim1$ for $k_y\neq0$, and all subsequent changes occur along the line $k_y=0$. There, the main peaks of $S(k_x,k_y=0)$ grow, while for lower wave vectors, $S(k_x,k_y=0)$ is basically unchanged from its equilibrium values. This is a

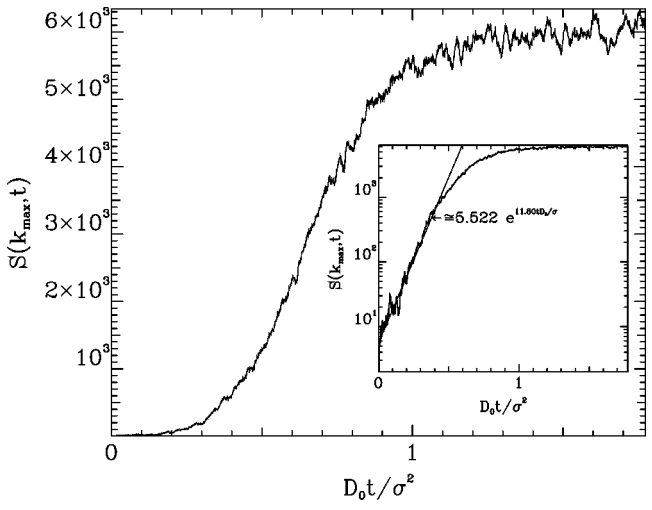

FIG. 6. The evolution of the peak maximum for the Langevin calculation shown in Fig. 5.

different outcome from what the perturbative calculation of [13] predicted, i.e. a flattening of $S(k_x,k_y=0)$, except in the neighborhood of the main peak. For wave vectors larger than the equilibrium main peak, large fluctuations preclude us from determining whether the structure factor in the shear gradient direction flattens or retains its equilibrium shape. Referring again to Fig. 5, after 4 to 5 diffusion times, stripes are discernible, and the peaks of $S(k_x,k_y=0)$ are now of the order of 1000. As the system evolves, the stripes become better defined and the peaks grow until saturation is reached. Then, after roughly 18 diffusion times, stripes are clearly seen, and the peaks of the structure factor have stopped growing, having reached a value of about 6000.

The structure factor in the gradient direction reveals another unexpected feature. Whereas the one-loop perturbation theory predicted that the main peak would shift to a smaller wave number (i.e., larger wavelengths) by as much as 20 to 30% as the instability is approached, Fig. 5 shows the growth in the structure factor occurring very close to the equilibrium main peak. The exact position remains uncertain because of the finite mesh size, but it is clearly very close to the equilibrium main peak. This is in agreement with the analysis of the moment equations, and is discussed in more detail in the Appendix.

In the flow direction (here the y direction), the structure factor flattens out, which means that under large shear, the system becomes almost perfectly disordered in the flow direction, cf. Fig. 5. This is in accord with the observation made in [13]; i.e., linear theory [24] is a good approximation as long as $\alpha k_y \gg 1$, and consequently, for large shear rates, nonlinearities are important only in the plane perpendicular to the velocity direction, with the system being strongly disordered elsewhere.

Figure 6 shows the evolution of the main peak with time. The inset, depicting the same data on a semilog plot, reveals that the long-range order develops following a single exponential growth until close to saturation. Furthermore, the slope of the semilog plot has roughly the same value as that found by the moments' method. That is, the growth evolves according to $\exp(t/\tau)$, where $10<1/\tau<12$. Note that while the Langevin approach seems to saturate, presumably because of higher-order mode-coupling effects than those considered in the moments approach, the saturation amplitude of the density modulation is quite large. This suggests that the model probably needs additional stabilizing terms such as higher-order nonlinear corrections associated with the chemical potential (which involve the higher-order direct correlation function) or with the Onsager coefficients themselves; neither of these quantities is known particularly well, and moreover would greatly increase the numerical effort required to solve the resulting equations. A phenomenological approach to this problem will be reported elsewhere.

When the system was left to run longer in the layered regime, the runs sometimes became numerically unstable to large fluctuations occurring within the stripes. To see if this was only a numerical artifact, the time step was reduced further, to $\Delta t=10^{-7}$, and the system was run for an additional diffusion time without incurring any instability. Hence, the stripe pattern seems to be a stable steady-state configuration, although it is hard to confirm because of the limited number of diffusion times we are able to sample at such small Δt's. It is also possible that we are encountering turbulence effects which prove to be unstable for our numerical scheme. Note that such effects were seen in experiments such as those of Ackerson *et al.* [11], in which ''. . . occasional plumes of disordered regions . . .'' were reported. For our stochastic simulations, the sudden occurrence of large fluctuations within a stripe might correspond to an initial turbulent state leading to the ''plumes'' mentioned above.

Finally, note that the moment analysis and the full Langevin simulations give very similar descriptions of the onset of the instability and of the initial growth of the pattern. They differ in that the former does not seem to stabilize (for reasons described above) and the latter does not exhibit any Goldstone mode sidebands, cf. Figs. 3 and 5. There are several possible explanations for this difference. First, this is a strongly driven nonequilibrium system and there is no *a priori* reason why Goldstone modes should be there, the *approximate* moment analysis notwithstanding. Another possibility is that the two calculations handle finite size effects in subtly different ways, leading to a quenching of these long-wavelength fluctuations in the Langevin approach. Finally, it is clear that the moment analysis is missing something, since it does not seem to stabilize; the resulting structure factors seem to diverge, and it is likely that there is a concomitant amplification of the sidebands. Hence, they may be there in the Langevin approach, but they may be too small to see.

IV. CONCLUSIONS

The main goal of this work was to determine whether the instability toward the formation of a lamellar phase predicted theoretically [13], is indeed present at the nonperturbative level for the model represented by Eqs. (1) and (2). This is confirmed either by numerical analysis of the moment or Langevin equations. Because of computing constraints, the stochastic simulations were performed on a two-dimensional grid, which precluded quantitative comparison with three-dimensional calculations. Still, many interesting qualitative comparisons were obtained. First and foremost, it was found that the model does indeed go through a phase transforma-

tion at high enough packing fraction and shear rate, to a new phase where colloidal particles align themselves in stripes along the flow direction. Hence, a simple continuity equation for the number density of colloidal particles coupled to the Navier-Stokes equation for the fluid velocity with an added active-mixing term (required by detailed balance, and with no adjustable parameters) reproduce many features seen in various experiments and simulations on colloidal suspensions. The Langevin simulations also reveal that apart from early times, long-range order develops as a single exponential growth, up to late times when saturation occurs.

This suggests the presence of the usual linear instability, and is revealed in the moments' method where the theory is reformulated in an approximate fashion into relatively simple diffusionlike equations for the first and second moments which represent the developing long-range order and the short-range order, respectively. We have shown that the infinite shear limit correction to the structure factor found earlier by different perturbative methods [13] is easily recovered within this approach. Again with the help of numerical integration on a grid, the deterministic moments' equations are studied. We find that in roughly a diffusion time, the nonlinear diffusion operators evolve towards a steady state in which an original band of unstable modes shrinks to a single grid point in k space, and that the value of the unstable mode corresponds to the single exponential growth rate seen in the Langevin simulations. Furthermore, as for the Langevin simulations, the wave number corresponding to the wavelength of the lamellar pattern corresponds almost exactly (as far as can be resolved on our grid) to the position of the main peak of the equilibrium structure factor, which is contrary to results of our previous theoretical analysis. Apart from their use in clarifying the single exponential growth (and maybe the chosen wavelength of the layers) the moments' equations are of limited use because the projection operator appearing in the integrands (a result of the assumed incompressibility of the fluid) make for the vanishing of the stabilizing nonlinear term once a periodic pattern develops. Higher-order corrections would thus be needed to cure this problem.

In effect, we have shown through numerical simulations that a model based on simple symmetries contains the essential ingredients to reproduce many features of sheared colloidal suspensions.

ACKNOWLEDGMENTS

A portion of this work was supported by the National Science and Engineering Research Council of Canada.

APPENDIX A: PERIODIC SYSTEMS

For spatially periodic states,

$$\langle N(\mathbf{k})\rangle=\sum_{\mathbf{G}}\ \langle N_{\mathbf{G}}\rangle(2\pi)^d\delta(\mathbf{k}-\mathbf{G}) \tag{A1}$$

and

$$s(\mathbf{k};\mathbf{k}')=\sum_{\mathbf{G}}\ s_{\mathbf{G}}((\mathbf{k}-\mathbf{k}')/2)(2\pi)^d\delta(\mathbf{k}+\mathbf{k}'-\mathbf{G}), \tag{A2}$$

where $\mathbf{G}$ is a reciprocal lattice vector for the periodic system and where $s(\mathbf{k};\mathbf{k}')$ is the structure factor introduced in Eq. (32). The discrete Fourier coefficients $\langle N_{\mathbf{G}}\rangle$ are obtained from $\langle N(\mathbf{r})\rangle$ in the usual manner, that is

$$\langle N_{\mathbf{G}}\rangle\equiv\int_v\frac{d\mathbf{r}}{v}e^{i\mathbf{G}\cdot\mathbf{r}}\langle N(\mathbf{r})\rangle, \tag{A3}$$

where v is the volume of the primitive lattice cell. Similarly,

$$s_{\mathbf{G}}(\mathbf{k})\equiv\int_v\frac{d\mathbf{R}}{v}\int_\infty d\mathbf{r}\,e^{i\mathbf{G}\cdot\mathbf{R}+i\mathbf{k}\cdot\mathbf{r}}s(\mathbf{R}+\tfrac{1}{2}\mathbf{r};\mathbf{R}-\tfrac{1}{2}\mathbf{r}), \tag{A4}$$

where $n_c s(\mathbf{r};\mathbf{r}')$ is the real-space, two-point density cumulant, cf. Eq. (32). Since $s(\mathbf{r};\mathbf{r}')$ is a symmetric function of $\mathbf{r}$ and $\mathbf{r}'$, it follows that $s_{\mathbf{G}}(\mathbf{k})$ is an even function of $\mathbf{k}$. Equation (A2) is tantamount to assuming that

$$s(\mathbf{r};\mathbf{r}')=F(\tfrac{1}{2}(\mathbf{r}+\mathbf{r}');\mathbf{r}-\mathbf{r}'), \tag{A5}$$

where $F(\mathbf{R};\mathbf{r})$ is periodic in $\mathbf{R}$ with the periodicity of the lattice.

The dimensionality of the reciprocal lattice can be less than that of the system, and in particular, we will assume that there is no order in the direction of the shear velocity (y), and thus, G_y vanishes. This has the effect of eliminating many of the shear convective terms. In order to see how this comes about for the variance, we let

$$\mathbf{K}\equiv\mathbf{k}+\mathbf{k}'\quad\text{and}\quad\boldsymbol{\kappa}\equiv(\mathbf{k}-\mathbf{k}')/2, \tag{A6}$$

from which it follows that

$$k_y\frac{\partial}{\partial k_x}+k_y'\frac{\partial}{\partial k_x'}=K_y\frac{\partial}{\partial K_x}+\kappa_y\frac{\partial}{\partial\kappa_x}. \tag{A7}$$

Thus, the factors of $\delta(\mathbf{k}+\mathbf{k}'-\mathbf{G})$ appearing in Eq. (A2) allow us to drop the convective terms in K_y when there is no periodicity in the y direction. On the other hand, the convection still acts on $\boldsymbol{\kappa}$, which, cf. Eq. (A5), corresponds to a relative coordinate.

By using Eqs. (A1) and (A2) in Eq. (17), in the Gaussian approximation, we find that

$$\frac{\partial\langle N_{\mathbf{G}}\rangle}{\partial t}=-\sum_{\mathbf{G}_1}\ \mathbf{\Gamma}_{\mathbf{G};\mathbf{G}_1}\langle N_{\mathbf{G}_1}\rangle-\frac{k_BT}{\eta}\sum_{\mathbf{G}_1,\mathbf{G}_2}\frac{\mathbf{G}\cdot\overleftrightarrow{\Phi}_{\mathbf{G}_1}\cdot\mathbf{G}_2}{\mathbf{G}_1^2n_cS^{(eq)}(\mathbf{G}_2)}\times\langle N_{\mathbf{G}-\mathbf{G}_1}\rangle\langle N_{\mathbf{G}_1-\mathbf{G}_2}\rangle\langle N_{\mathbf{G}_2}\rangle, \tag{A8}$$

where

$$\Gamma_{\mathbf{G};\mathbf{G}} \equiv \frac{D_{SE}G^2}{S^{(eq)}(G)} + \frac{k_BT}{\eta}\int \frac{d\mathbf{k_1}}{(2\pi)^d}\frac{\mathbf{G}\cdot\vec{\Phi}_{\mathbf{k_1}}\cdot\mathbf{G}}{k_1^2} \times\left[s_{\mathbf{0}}(\mathbf{G}-\mathbf{k}_1)\left(\frac{1}{S^{(eq)}(G)} - \frac{1}{S^{(eq)}(|\mathbf{G}-\mathbf{k}_1|)}\right) + 1 - \frac{1}{S^{(eq)}(G)}\right] \tag{A9a}$$

and

$$\Gamma_{\mathbf{G};\mathbf{G}_1} \equiv \frac{k_BT}{\eta}\int \frac{d\mathbf{k_1}}{(2\pi)^d}\left[\frac{\mathbf{G}\cdot\vec{\Phi}_{\mathbf{G}-\mathbf{G}_1}\cdot\mathbf{k}_1}{|\mathbf{G}-\mathbf{G}_1|^2 S^{(eq)}(k_1)} \times s_{\mathbf{G}-\mathbf{G}_1}(\mathbf{k}_1-(\mathbf{G}-\mathbf{G}_1)/2) + \frac{\mathbf{G}\cdot\vec{\Phi}_{\mathbf{k_1}}\cdot\mathbf{G}_1}{k_1^2} s_{\mathbf{G}-\mathbf{G}_1}((\mathbf{G}+\mathbf{G}_1)/2-\mathbf{k}_1) \times\left(\frac{1}{S^{(eq)}(G_1)} - \frac{1}{S^{(eq)}(|\mathbf{G}_1-\mathbf{k}_1|)}\right)\right] \quad \text{for } \mathbf{G}\neq\mathbf{G}_1, \tag{A9b}$$

where we have also introduced D_{SE}, cf. Eq. (22). Note that the diagonal part of Γ is equivalent to the diffusion operators obtained in the text; i.e., $\Gamma_{\mathrm{G;G}}=\Gamma(\mathbf{G},t)$, cf. Eq. (26). Also note that the nonlinear terms vanish for one-dimensional patterns; this has some interesting implications for two-dimensional systems, as discussed in the text.

By using Eqs. (A1) and (A2) in the general second moment equations, cf. Eq. (18), and making the Gaussian approximation, it follows that

$$\begin{aligned}
\frac{\partial s_{\mathbf{G}}(\mathbf{k})}{\partial t} &= \omega_0 k_y \frac{\partial s_{\mathbf{G}}(\mathbf{k})}{\partial k_x} + \left\{\left[-\frac{D_{SE}|\frac{1}{2}\mathbf{G}+\mathbf{k}|^2}{S^{(eq)}(|\frac{1}{2}\mathbf{G}+\mathbf{k}|)} - \frac{k_BT}{\eta}\int \frac{d\mathbf{k}_1}{(2\pi)^d}\frac{(\frac{1}{2}\mathbf{G}+\mathbf{k}):\vec{\Phi}_{\mathbf{k}_1}(\frac{1}{2}\mathbf{G}+\mathbf{k})}{k_1^2}\left(1-\frac{1}{S^{(eq)}(|\frac{1}{2}\mathbf{G}+\mathbf{k}|)}\right)\right] s_{\mathbf{G}}(\mathbf{k})\right. \\
&- \frac{k_BT}{\eta}\left[\sum_{\mathbf{G}_1,\mathbf{G}_2}\frac{(\frac{1}{2}\mathbf{G}+\mathbf{k})(-\frac{1}{2}\mathbf{G}+\mathbf{k}+\mathbf{G}_2):\vec{\Phi}_{(-1/2)\mathbf{G}+\mathbf{k}+\mathbf{G}_1}}{|-\frac{1}{2}\mathbf{G}+\mathbf{k}+\mathbf{G}_1|^2 n_c S^{(eq)}(|-\frac{1}{2}\mathbf{G}+\mathbf{k}-\mathbf{G}_2|)}\langle N_{\mathbf{G}-\mathbf{G}_1}\rangle\langle N_{\mathbf{G}_1-\mathbf{G}_2}\rangle s_{\mathbf{G}_2}(\mathbf{k}-\tfrac{1}{2}(\mathbf{G}-\mathbf{G}_2))\right. \\
&+ \sum_{\mathbf{G}_1,\mathbf{G}_2}\frac{(\frac{1}{2}\mathbf{G}+\mathbf{k})(\mathbf{G}_1-\mathbf{G}_2):\vec{\Phi}_{-\frac{1}{2}\mathbf{G}+\mathbf{k}+\mathbf{G}_1}}{|-\frac{1}{2}\mathbf{G}+\mathbf{k}+\mathbf{G}_1|^2 n_c S^{(eq)}(|\mathbf{G}_1-\mathbf{G}_2|)}\langle N_{\mathbf{G}-\mathbf{G}_1}\rangle\langle N_{\mathbf{G}_1-\mathbf{G}_2}\rangle s_{\mathbf{G}_2}(\mathbf{k}-\tfrac{1}{2}(\mathbf{G}-\mathbf{G}_2)) \\
&+ \sum_{\mathbf{G}_1,\mathbf{G}_2}\frac{(\frac{1}{2}\mathbf{G}+\mathbf{k})(\mathbf{G}_1-\mathbf{G}_2):\vec{\Phi}_{\mathbf{G}-\mathbf{G}_2}}{|\mathbf{G}-\mathbf{G}_2|^2 n_c S^{(eq)}(|\mathbf{G}_1-\mathbf{G}_2|)}\langle N_{\mathbf{G}-\mathbf{G}_1}\rangle\langle N_{\mathbf{G}_1-\mathbf{G}_2}\rangle s_{\mathbf{G}_2}(\mathbf{k}-\tfrac{1}{2}(\mathbf{G}-\mathbf{G}_2)) \\
&+ \sum_{\mathbf{G}_1}\int\frac{d\mathbf{k}_1}{(2\pi)^d}\frac{(\frac{1}{2}\mathbf{G}+\mathbf{k})(-\frac{1}{2}\mathbf{G}+\mathbf{k}+\mathbf{G}_1):\vec{\Phi}_{\mathbf{k}_1}}{k_1^2 S^{(eq)}(|-\frac{1}{2}\mathbf{G}+\mathbf{k}+\mathbf{G}_1|)}s_{\mathbf{G}_1}(\mathbf{k}-\mathbf{k}_1+\tfrac{1}{2}(\mathbf{G}-\mathbf{G}_1))s_{\mathbf{G}-\mathbf{G}_1}(\mathbf{k}+\tfrac{1}{2}(\mathbf{G}_1+\mathbf{G})) \\
&+ \sum_{\mathbf{G}_1}\int\frac{d\mathbf{k}_1}{(2\pi)^d}\frac{(\frac{1}{2}\mathbf{G}+\mathbf{k})(-\frac{1}{2}\mathbf{G}-\mathbf{k}+\mathbf{k}_1+\mathbf{G}_1):\vec{\Phi}_{\mathbf{k}_1}}{k_1^2 S^{(eq)}(|-\frac{1}{2}\mathbf{G}-\mathbf{k}+\mathbf{k}_1+\mathbf{G}_1|)}s_{\mathbf{G}_1}(\mathbf{k}-\mathbf{k}_1+\tfrac{1}{2}(\mathbf{G}-\mathbf{G}_1))s_{\mathbf{G}-\mathbf{G}_1}(\mathbf{k}+\tfrac{1}{2}\mathbf{G}_1) \\
&+ \left.\left.\sum_{\mathbf{G}_1\neq\mathbf{G}}\int\frac{d\mathbf{k}_2}{(2\pi)^d}\frac{(\frac{1}{2}\mathbf{G}+\mathbf{k})\mathbf{k}_2:\vec{\Phi}_{\mathbf{G}-\mathbf{G}_1}}{|\mathbf{G}-\mathbf{G}_1|^2 S^{(eq)}(k_2)}s_{\mathbf{G}_1}(\mathbf{k}-\tfrac{1}{2}(\mathbf{G}-\mathbf{G}_1))s_{\mathbf{G}-\mathbf{G}_1}(\tfrac{1}{2}(\mathbf{G}-\mathbf{G}_1)-\mathbf{k}_2)\right]\right. \\
&\left. - \frac{k_BT}{\eta}\sum_{\mathbf{G}_1}\frac{(\frac{1}{2}\mathbf{G}+\mathbf{k})(\frac{1}{2}\mathbf{G}-\mathbf{k}):\vec{\Phi}_{(1/2)\mathbf{G}+\mathbf{k}-\mathbf{G}_1}}{n_c|\frac{1}{2}\mathbf{G}+\mathbf{k}-\mathbf{G}_1|^2}\langle N_{\mathbf{G}-\mathbf{G}_1}\rangle\langle N_{G_1}\rangle\right\} + \{\mathbf{k}\leftrightarrow-\mathbf{k}\} + 2D_{SE}k^2\delta_{\mathbf{G},0} \\
&- \frac{2k_BT}{\eta}\int\frac{d\mathbf{k}_1}{(2\pi)^d}\frac{(\frac{1}{2}\mathbf{G}+\mathbf{k})(\frac{1}{2}\mathbf{G}-\mathbf{k}):\vec{\Phi}_{\mathbf{k}_1}}{k_1^2}[s_{\mathbf{G}}(\mathbf{k}-\mathbf{k}_1)-\delta_{\mathbf{G},0}],
\end{aligned} \tag{A10}$$

where Eq. (22) has again been used. If we assume that $s_{\mathbf{G}}(\mathbf{k})=0$ for nonzero $\mathbf{G}$, Eq. (A10) becomes

$$\frac{\partial s_0(\mathbf{k})}{\partial t}=\omega_0 k_y\frac{\partial s_0(\mathbf{k})}{\partial k_x}-2\Gamma_0(\mathbf{k},t)s_0(\mathbf{k})+2\mathcal{N}_0(\mathbf{k},t), \tag{A11}$$

where

$$\Gamma_0(\mathbf{k},t)\equiv\frac{D_{SE}k^2}{S^{(eq)}(k)}+\frac{k_BT}{\eta}\int\frac{d\mathbf{k}_1}{(2\pi)^d}\frac{\mathbf{kk}:\overleftrightarrow{\Phi}_{\mathbf{k}_1}}{k_1^2}\times\left[s_0(\mathbf{k}-\mathbf{k}_1)\left(\frac{1}{S^{(eq)}(k)}-\frac{1}{S^{(eq)}(|\mathbf{k}-\mathbf{k}_1|)}\right)+1-\frac{1}{S^{(eq)}(k)}\right]+\frac{k_BT}{\eta}\sum_{\mathbf{G}_1}\frac{\mathbf{kk}:\overleftrightarrow{\Phi}_{\mathbf{k}-\mathbf{G}_1}}{|\mathbf{k}-\mathbf{G}_1|^2n_c}\times|\langle N_{\mathbf{G}_1}\rangle|^2\left(\frac{1}{S^{(eq)}(k)}-\frac{1}{S^{(eq)}(G_1)}\right) \tag{A12a}$$

and where

$$\mathcal{N}_0(\mathbf{k},t)\equiv D_{SE}k^2+\frac{k_BT}{\eta}\int\frac{d\mathbf{k}_1}{(2\pi)^d}\frac{\mathbf{kk}:\overleftrightarrow{\Phi}_{\mathbf{k}_1}}{k_1^2}[s_0(\mathbf{k}-\mathbf{k}_1)-1]+\frac{k_BT}{\eta}\sum_{\mathbf{G}_1}\frac{\mathbf{kk}:\overleftrightarrow{\Phi}_{\mathbf{k}-\mathbf{G}_1}}{n_c|\mathbf{k}-\mathbf{G}_1|^2}|\langle N_{\mathbf{G}_1}\rangle|^2. \tag{A12b}$$

For disordered states, $\langle N_{\mathbf{G}}\rangle$ vanishes, and the noise and relaxation rate are identical to those introduced in the text, cf. Eqs. (27) and (26). In addition, if we take the continuum limit, i.e., we let $\Sigma_{\mathbf{G}_1}\to V\int d\mathbf{G}/(2\pi)^d$ and $\langle N_{\mathbf{G}}\rangle\to\langle N(\mathbf{G})\rangle/V$, we obtain Eq. (34).

There are several conclusions that can be drawn from the approximate equations of motion for the first two moments, Eqs. (A8) and (A11). First, notice that the sum over wave numbers in Eq. (A12a) can diverge as k approaches a reciprocal lattice vector, and perhaps more problematically, the divergent terms will be both positive and negative depending on the direction of approach. One way that this can be avoided entirely is that the reciprocal lattice vectors have a magnitude corresponding to an extremum of the equilibrium structure factor. In this event, the divergence disappears and the corresponding term in the sum in Eq. (A12a) becomes

$$\frac{k_BTG_1^2|\langle N_{\mathbf{G}_1}\rangle|^2}{8\eta n_c}\left(\frac{\partial^2[S^{(eq)}(k)]^{-1}}{\partial k^2}\right)_{k=G_1}\sin^2(2\theta), \tag{A13}$$

as $\mathbf{k}\to\mathbf{G}_1$, where θ is the angle between $\mathbf{k}-\mathbf{G}_1$ and $\mathbf{G}_1$. The term now has a definite sign, and in particular is positive when G_1 corresponds to a minimum of the equilibrium structure factor. Indeed, our numerical work confirms these predictions, cf., e.g., Fig. 4.

While the preceding argument suggests that any pattern should arise with a characteristic wave vector corresponding to the main structural peak of the equilibrium structure factor, it is by no means a proof, nor does it imply that a steady state exists. In particular, the nonlinear terms in Eq. (A8) vanish identically for one-dimensional patterns, and hence, for the two-dimensional numerical studies presented in the text. Thus, the existence of a steady state implies that either $\Gamma_{\mathbf{G}_1,\mathbf{G}_1}=0$, cf. Eq. (A9a) or that other nonlinearities be introduced, either as corrections to the Gaussian approximations used to analyze the Fokker-Planck equation, or as corrections to the model.

If a steady state exists, we can formally solve Eq. (A10), thereby obtaining the same forms as found in Eq. (28), with $\Gamma_0(\mathbf{k},t)$ and $\mathcal{N}_0(\mathbf{k},t)$ substituted for $\Gamma(\mathbf{k})$ and $\mathcal{N}(\mathbf{k})$, respectively. (Of course, for this to work, we require that $\Gamma_0(\mathbf{k},t)>0$ when $k_y=0$). The discrete terms in $\mathcal{N}_0(\mathbf{k},t)$ are interesting; they diverge when $\mathbf{k}$ approaches a reciprocal lattice vector, and while this divergence will be smeared out by the integrations over k_x in Eq. (28), it will become more and more important as $k_y\to0$. Indeed, for $k_y=0$ we can use Eq. (29) and conclude that $s_0(\mathbf{k})$ is $|\mathbf{k}-\mathbf{G}_1|^{-2}$ singular in the $k_y=0$ plane. This is not totally surprising, and is reminiscent of the Goldstone-mode singularities caused by phonons in crystals [39], although here the shear makes them very anisotropic. More generally, for k_y sufficiently small, we can ignore the effects of convection, and hence, Eq. (A12b) suggests that

$$s_0(\mathbf{k})\propto\frac{\sin^2(\theta)}{|\mathbf{k}-\mathbf{G}_1|^{2-\eta}}, \tag{A14}$$

where the exponent η will be nonzero if $\Gamma_0(\mathbf{G}_1,t)\sim|\mathbf{k}-\mathbf{G}_1|^{\eta}$ as $\mathbf{k}\to\mathbf{G}_1$. Our numerical work suggests that $0.5\leqslant-\eta\leqslant1$.

[1] R. Hoffman, Trans. Soc. Rheol. **16**, 155 (1972).
[2] J. Erpenbeck, Phys. Rev. Lett. **52**, 1333 (1984).
[3] L. Woodcock, Phys. Rev. Lett. **54**, 1513 (1985).
[4] D. Heyes, G. Morriss, and D. Evans, J. Chem. Phys. **83**, 4760 (1985).
[5] M. Stevens, M. Robbins, and J. Belak, Phys. Rev. Lett. **66**, 3004 (1991).
[6] W. Xue and G. Grest, Phys. Rev. Lett. **64**, 419 (1990).
[7] S. Rastogi, N. Wagner, and S. R. Lustig, J. Chem. Phys. **104**, 9234 (1996).
[8] P. Mitchell and D. Heyes, Mol. Simul. **15**, 361 (1995).
[9] D. Ronis and S. Khan, Phys. Rev. A **41**, 6813 (1990).
[10] J.-Y. Yuan and D. Ronis, Phys. Rev. E **48**, 2880 (1993).
[11] B. Ackerson, J. Hayter, N. Clark, and L. Cotter, J. Chem. Phys. **84**, 2344 (1986).
[12] J. Bender and N. Wagner, J. Rheol. **40**, 899 (1996).

[13] B. Morin and D. Ronis, Phys. Rev. E **54**, 576 (1996).
[14] U. Deker and F. Haake, Phys. Rev. A **11**, 2043 (1975).
[15] H. Janssen, in *Lecture Notes in Physics*, edited by C. Enz (Springer, Berlin, 1979), Vol. 104, p. 1.
[16] L. Kadanoff and J. Swift, Phys. Rev. **166**, 89 (1968).
[17] J. Swift, Phys. Rev. **157**, 257 (1968).
[18] K. Kawasaki, Ann. Phys. (N.Y.) **61**, 1 (1970).
[19] B. Halperin, P. Hohenberg, and E. Siggia, Phys. Rev. Lett. **32**, 1289 (1974).
[20] E. Siggia, B. Halperin, and P. Hohenberg, Phys. Rev. B **13**, 2110 (1976).
[21] P. Hohenberg and B. Halperin, Rev. Mod. Phys. **49**, 435 (1977).
[22] R. Ruiz and D. Nelson, Phys. Rev. A **23**, 3224 (1981).
[23] P.-G. de Gennes, Physica (Utrecht) **25**, 825 (1959).
[24] D. Ronis, Phys. Rev. A **29**, 1453 (1984).
[25] L. D. Landau and E. M. Lifshitz, in *Fluid Mechanics* (Pergamon, London, 1959), Chap. 20.
[26] E. Helfand and G. Fredrickson, Phys. Rev. Lett. **62**, 2468 (1989).
[27] A. Onuki, Phys. Rev. Lett. **62**, 2472 (1989).
[28] D. Ronis, Phys. Rev. A **34**, 1472 (1986).
[29] T. Keyes, in *Statistical Mechanics Part B: Time-Dependent Processes*, edited by B. Berne (Plenum, New York, 1977), and references therein.
[30] C. Beenakker, Physica A **128**, 48 (1984).
[31] M. Kops-Werkhoven and H. Fijnaut, J. Chem. Phys. **77**, 2242 (1982).
[32] A. van Blaaderen, J. Peetermans, G. Maret, and J. Dhont, J. Chem. Phys. **96**, 4591 (1992).
[33] C. Pyun and M. Fixman, J. Chem. Phys. **41**, 937 (1964).
[34] G. Batchelor, J. Fluid Mech. **52**, 245 (1972).
[35] A. Altenberger and J. Deutch, J. Chem. Phys. **59**, 894 (1973).
[36] E. Helfand, Bell Syst. Tech. J. **58**, 2239 (1979).
[37] H. Greenside and E. Helfand, Bell Syst. Tech. J. **60**, 95 (1981).
[38] P. Kloeden and E. Platen, *Numerical Solution of Stochastic Differential Equations* (Springer, New York, 1995).
[39] H. Wagner, Z. Phys. **195**, 273 (1966).